Consequences of three-dimensional physical and electromagnetic structures on dust particle trapping in high plasma density material processing discharges

Helen H. Hwang,[a] Eric R. Keiter,[b] and Mark J. Kushner[c]
Department of Electrical and Computer Engineering, University of Illinois, Urbana, Illinois 61801

Plasma processing discharges are typically designed with the goal of having uniform reactant fluxes to the substrate and a minimum of dust particle contamination of the wafer. It is not uncommon, however, that reactors have three-dimensional (3D) structures such as antennas (or coils), gas injection nozzles, sub- or super-wafer topography and single-sided pump ports. These structures can contribute to azimuthal asymmetries in reactant fluxes. These structures may also produce dust particle traps. In this paper, a 3D plasma equipment model is applied to investigate the impact of these structures on reactant fluxes and their influence on dust particle trapping in inductively coupled radio frequency discharges under conditions where trapping is not typically obtained. We find that 3D structures, such as injection nozzles, perturb the plasma potential and ion fluxes to distances well beyond their geometrical boundaries. These perturbations are sufficient to create dust particle traps. Electromagnetic asymmetries caused by coils which have poor impedance matching may also produce sufficient azimuthal asymmetries in ion fluxes that dust particle traps are generated. © *1998 American Vacuum Society.* [S0734-2101(98)04804-0]

I. INTRODUCTION

Optimizing the yield of devices during plasma processing of microelectronics requires controlling defects generated by particle contamination. Investigation of dust particle transport in low pressure plasma processing discharges therefore continues to be of interest.[1] Laser light scattering measurements of dust particles in these devices have revealed that trapping dominantly occurs near the plasma-sheath boundary where electrostatic and ion-drag forces on the negatively charged dust particles are in balance. In azimuthally symmetric parallel plate capacitively coupled discharges, these trapping sites typically form a single uniform plane, although Coulomb particle–particle interactions may thicken the dust particle sheet at high particle densities.[2,3] Trapping of particles in rings around and domes above wafers in reactive ion etching (RIE) discharges has been observed, as have dust particle traps which have been generated by protruding rings or grooves.[4,5] All of those observations can be explained, to first order, by perturbations in the plasma potential and ion flux which shift the spatial location of equilibrium between the ion drag and electrostatic forces. When gas flow or temperature gradients are present, which introduce fluid drag and thermophoretic forces, dust particle traps may be shifted or disrupted by the addition of these accelerations.[6]

It is unusual to find dust particle traps in low pressure, high plasma density reactors, such as electron cyclotron resonance, helicon and inductively coupled plasma (ICP) devices

due to the large ion flux which produces large ion drag forces, and the low gas pressure which results in low fluid drag forces.[7,8] The large ion drag forces produce large expulsion accelerations while the confining sheath electric fields are typically small compared to RIE devices. When applying a radio frequency (rf) bias to the substrate, the confining electric fields in the sheath are increased and contamination of the wafer is reduced.[8] Particle trapping at sheath edges may also occur at, for example, high rf bias powers and low inductively coupled power deposition.[9,10]

It is certainly the goal of reactor design to have radially and azimuthally uniform reactant fluxes to the substrate. Many experimental and two-dimensional (2D) modeling studies have quantified the consequences of nonuniformities in plasma sources and reactor geometry on the radial uniformity of reactant densities and fluxes to the substrates. For example, electric field enhancement at the edge of electrodes in RIE systems have been correlated with local radial maxima in excited state and plasma densities[11] The location of the coil in ICP systems has been well correlated with the radial uniformity of reactant fluxes.[12–14] Observations of azimuthal asymmetries in etch characteristics have been correlated or attributed to nonuniform gas injection and pumping, geometrical structures such as injection nozzles and, in the case of ICP systems, transmission line effects in the antenna.[15] The issue we wish to address in this paper is whether these azimuthal asymmetries in reactant fluxes can produce dust particle traps in high plasma density systems which would otherwise be free of traps.

A three-dimensional (3D) plasma equipment model has been used to investigate the consequences of geometrical structures such as gas injection nozzles, and electrical structures such as transmission lines, on the generation of dust

particle traps in ICP reactors. Results from that investigation will be reported here. We found that both physical and electromagnetic asymmetries in these reactors can induce dust particle traps by perturbing ion fluxes and the plasma potential. The models we have used in this study are described in Sec. II followed by a discussion of our results for 3D particle trapping in Sec. III. Our concluding remarks are in Sec. IV.

II. DESCRIPTION OF THE MODEL

The models we have used in this study are a 3D plasma equipment model and a 3D dust particle transport simulation. The modeling sequence begins by obtaining plasma properties in the absence of dust particles using a model we call the hybrid plasma equipment model (HPEM-3D).[16] The plasma model generates time averaged electric fields, electron and ion densities, electron temperatures and heavy particle fluxes. These quantities are subsequently used by the dust transport simulation (DTS-3D) in which the trajectories of dust particles are integrated in time. For these calculations, we are addressing particle densities which are sufficiently small that they do not significantly perturb the plasma properties, and so results from DTS-3D are not fed back to the plasma equipment model.

The HPEM-3D, as used in this study, is described in detail in Ref. 16. HPEM-3D consists of three major modules. The electromagnetic module (EMM) produces the amplitude and phase of inductively coupled fields as a function of (r, θ, z). These fields are then used in the electron energy equation module (EEM) which solves for the average electron energy as a function of position. These values are used to calculate electron transport coefficients and electron impact source functions for inelastic collisional processes. The electron transport coefficients and source functions are subsequently used in the fluid-kinetics module (FKM) where species densities and momenta are obtained, and Poisson's equation is solved for the electrostatic potential. The resulting densities, electric fields and conductivities are cycled back to the EMM and EEM; and the sequence is repeated until quasi-steady state conditions are obtained. The version of HPEM-3D used in the present study is functionally the same as that described in Ref. 16 except that a new computational acceleration technique was employed to speed the convergence. This acceleration technique entails solving for the electric potential using an ambipolar approximation based on a Poisson-like formulation. The ambipolar derived fields are used until species densities reach near their steady state values. At that time we switch to obtaining the electric potential by directly solving Poisson's equation. Details of this acceleration technique will be described in an upcoming publication.

DTS-3D is functionally equivalent to the two-dimensional DTS described in Ref. 3. Given the 3D electric fields, species densities, fluxes and temperatures from HPEM-3D, transport equations for dust particles are formulated. The forces we consider are gravity, electrostatic, ion drag, neutral fluid drag and thermophoresis. The charge on the dust particles is as-

sumed to be in equilibrium with the local electron and ion densities, fluxes and temperatures, and is computed using the technique described in Ref. 6. Particles of a selected size and mass density are initially uniformly distributed in the reactor, and their trajectories are computed until they strike a surface, are trapped or the simulation time is exceeded (typically 0.1–1 s). Statistics are gathered on final particle locations, collection of particles on surfaces, and on the volumetric fluence. Additional bursts of particles are often employed to reduce statistical noise in the data. Acceptable statistics in three-dimensions are usually obtained using 50 000–100 000 particles. In order to reduce computing time, a short past history of the locations of particles is retained. If a particle's position has not changed by at least a specified amount over, for example, 0.1 s, then the particle is declared ''trapped.'' The trapping location is recorded and the particle is removed from the simulation.

III. REACTANT FLUXES AND PARTICLE TRAPS IN REACTORS WITH 3D STRUCTURES

In this section we will discuss the consequences of 3D structures on the formation of particle traps with special emphasis on those traps formed above or in the close vicinity of the wafer. It is a reasonable to expect that particle traps above the wafer are, in some quantitative way, worse with respect to wafer contamination than particle traps near the walls or particle accumulation on the walls. It is important to point out, however, that even though particle trapping above the wafer may be more of an immediate problem, particle trapping near the walls of the reactor, which results in the continued buildup of particles on the walls, also substantially contributes to contamination of the wafer. This contamination results from subsequent fracture of the coating and particle release. This buildup of particle contamination necessitates opening, physical cleaning and reconditioning of the reactor. In general, any particle trapping is undesirable.

We first investigated the consequences of injection nozzles on reactant fluxes and the generation of particle traps in an ICP reactor. The test geometry, shown in Fig. 1, is an ICP reactor powered by a flat coil set on a dielectric window. The substrate is sized for a 20 cm diam wafer. Geometrical asymmetries are in the form of a load-lock bay and four metal gas injection nozzles which project to the edge of the wafer. To minimize the additional asymmetries which may result from transmission line effects in the antenna,[15] we specified that the coil be two nested annuli whose conduction currents are uniform along their entire length. The base case conditions are an argon gas fill at 10 mTorr and 100 W inductive power deposition at 13.56 MHz. The dust particle mass density is 2.33 g cm^{-3}.

The plasma potential and ion density for Ar at 10 mTorr and 600 W inductive power deposition are shown in Figs. 2 and 3. Values are shown in the (r, θ) plane at the three axial locations shown in Fig. 1 (0.5 cm below the window, at the plane of the nozzles and at the plane of the substrate). The peak ion density is 3.8×10^{11} cm^{-3}, the peak plasma poten-
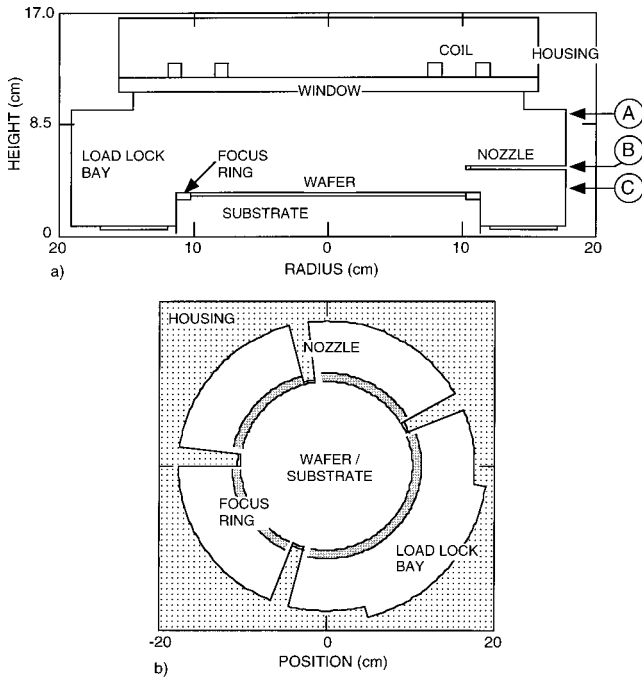
FIG. 1. Schematic of the flat-coil ICP reactor having injection nozzles used in this study: (a) side view, (b) view looking down on the substrate from below the window. The four nozzles extend to the edge of the wafer. The arrows in the top figure indicate the heights at which (r,θ) "slices" of plasma properties will be viewed.

FIG. 2. Plasma potential for an Ar discharge at 10 mTorr in the (r,θ) plane at the heights indicated in Fig. 1: (a) Below the window (height A of Fig. 1), (b) at the nozzles (height B), and (c) above the wafer (height C). Contours are labeled with the percentage of the maximum value shown in each figure. The plasma potential is perturbed many cm from the nozzles.

tial is 15.4 V and the maximum electron temperature is 4.1 eV. The metal injection nozzles pin the plasma potential to ground, thereby producing local maxima in the plasma potential between the nozzles. Unexpected, though, is the fact that the plasma potential is perturbed to both the height of the window and to the plane of the wafer. The local maxima in plasma potential between the nozzles are important with respect to dust particle trapping because the negatively charged particles will be attracted to the local peaks in plasma potential.

The ion density is similarly perturbed by the nozzles. The ion density is depressed at the height of the nozzle due to the recombination on their surfaces. An unexpected result is that the ion densities retain "scalloping" induced by the nozzles at both the height of the window and the lower level of the substrate. This scalloping is caused, to first order, from the ion loss to the nozzles resulting from recombination. To second order, the scalloping is caused by a shadowing effect. In flat coil ICP reactors, the electron impact ion source is dominantly near the top of the reactor within a few cm (the electromagnetic skin depth) of the window. The ion flux therefore dominantly originates above the nozzles and is shadowed by the nozzles in traversing the reactor to the substrate.

Dust particle locations are shown in Fig. 4 0.2 s after release for a reactor which is azimuthally symmetric (i.e., without nozzles or load-lock bay). The conditions are Ar at 10 mTorr, 200 W inductively coupled power and 1 μm diam particles. The view in Fig. 4(a) is a "plan view" from the
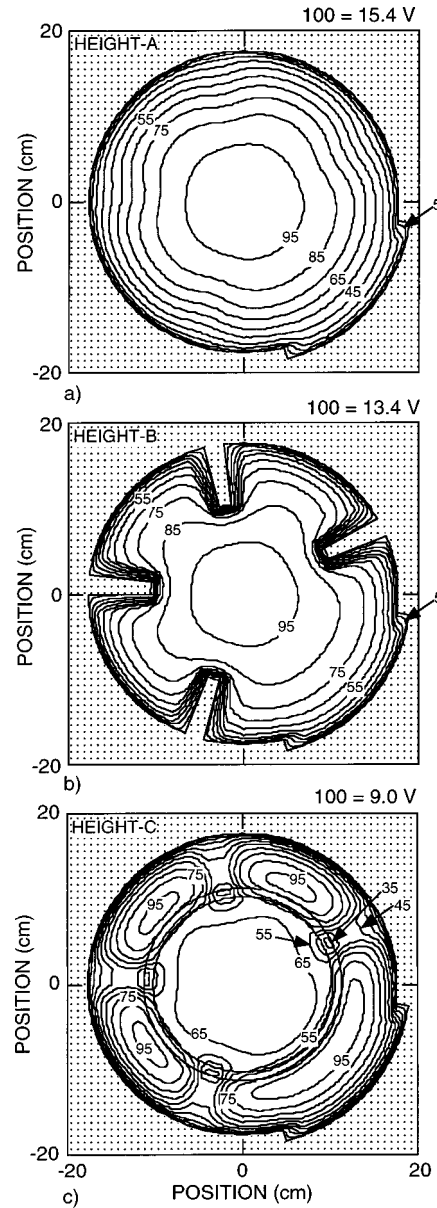
top of the reactor. The view in Fig. 4(b) is a cut-away in which roughly half the reactor is visible. With the exception of a few errant particles, there is no particle trapping in the center regions of the reactor. After dispersal, dust particles were accelerated by the large ion drag forces through the sheaths and were collected on surfaces. The only significant particle trapping occurs in the upper and lower corners of the reactor. At these locations the ion flux has been reduced by diffusion losses to a sufficient degree that the weak sheath electric fields are able to provide a counter balancing force.

Plan views (from the top of the reactor) of dust particle locations at various times after their release are shown in Fig.
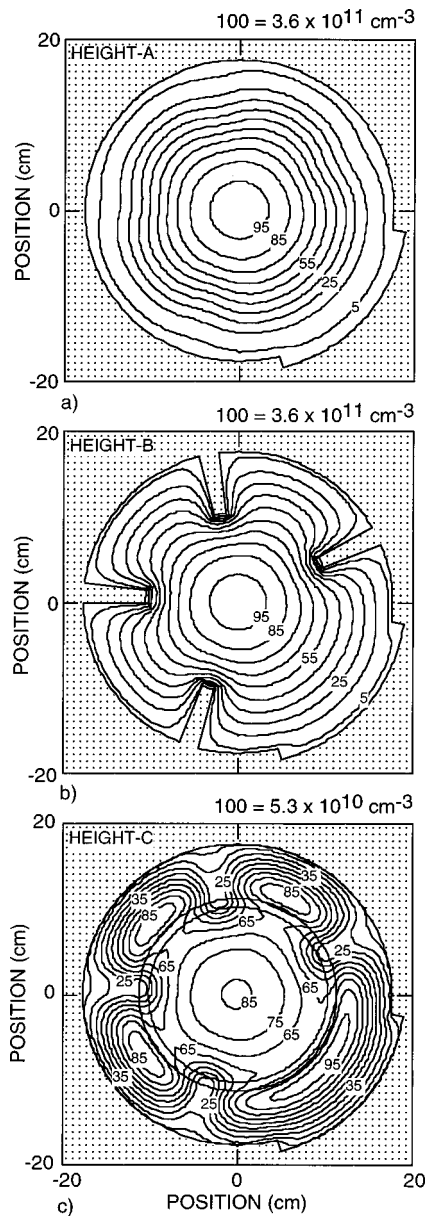
FIG. 3. Ion density for an Ar discharge at 10 mTorr in the (r, θ) plane at the heights indicated in Fig. 1: (a) below the window (height A of Fig. 1), (b) at the nozzles (height B), and (c) above the wafer (height C). Contours are labeled with the percentage of the maximum value shown in each figure. The ion density is significantly perturbed near the wafer due to both recombination on the nozzles and a shadowing of ion sources at higher heights.

FIG. 4. Particle locations (1 μm diameter) in an ICP reactor without nozzles: (a) plan view from the top and (b) cut-away view. Particle traps occur only in the peripheries and corners of the reactor where ion fluxes have decayed to low values.

5 for a reactor with nozzles and the load-lock bay. A cut-away view of the particle locations at 175 ms (essentially the steady state) is shown in Fig. 6. The power deposition is 100 W and the particle diameter is 1 μm. Upon their release, there is an initial burst of particles lost to surfaces as ion drag accelerates them through the sheaths. As time progresses, however, the remaining particles begin to segregate into three regions. The first region is along spokes aligned with the azimuth of the nozzles. The second is at an azimuth midway between the nozzles. The third is across a broad azimuth corresponding to the loadlock bay. The particles
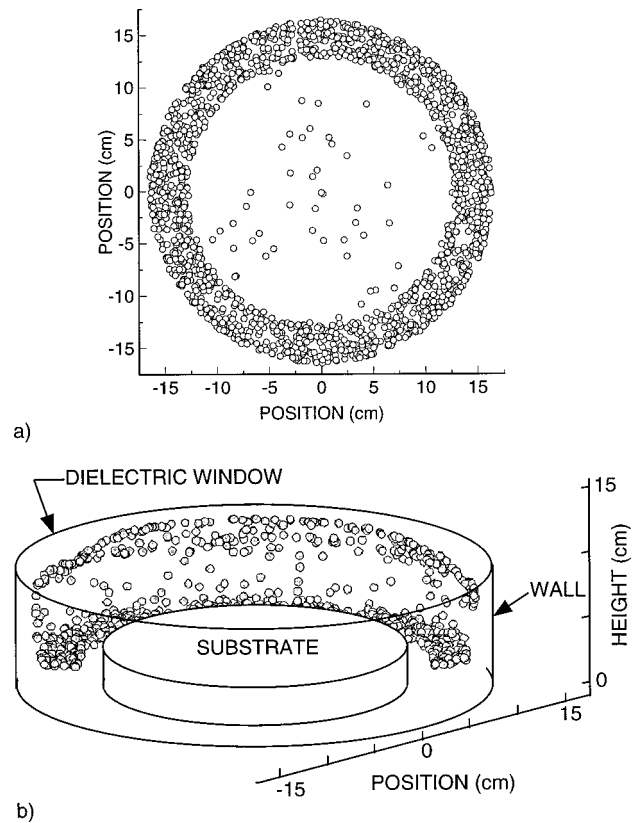
aligned with the nozzles are in narrow traps directly above and below the nozzles. The presence of the nozzles reduces the local diffusion length for loss of ions, which reduces the ion flux and increases the ambipolar electric field. These trends increase the likelihood for trapping particles by reducing the expulsionary ion drag force and increasing the counter balancing electrostatic force. The particle trap between the nozzles is broader in extent and shallower in depth. The trapping in these locations is correlated with a local minima in the ion drag forces and local maximum in plasma potential. The net ion flux at those locations is radially outward towards the walls and, due to the recombination on surfaces of the nozzles, towards the nozzles. As a result, there is a local minimum in the ion flux in between the nozzles which, combined with the local maximum in plasma potential, produces a trap.

The likelihood for inducing traps by structures such injection nozzles decreases with increasing power deposition and increases with increasing pressure. The former trend results from the increase in ion drag forces which accelerates dust particles through the traps, and the latter trend results from the increasing fluid drag forces which slows the particles. For example, plan views of dust particle locations are shown in Fig. 7(a) when operating at 100 mTorr with a power of 100 W; and in Figs. 7(b) and 7(c) for operating at 10 mTorr
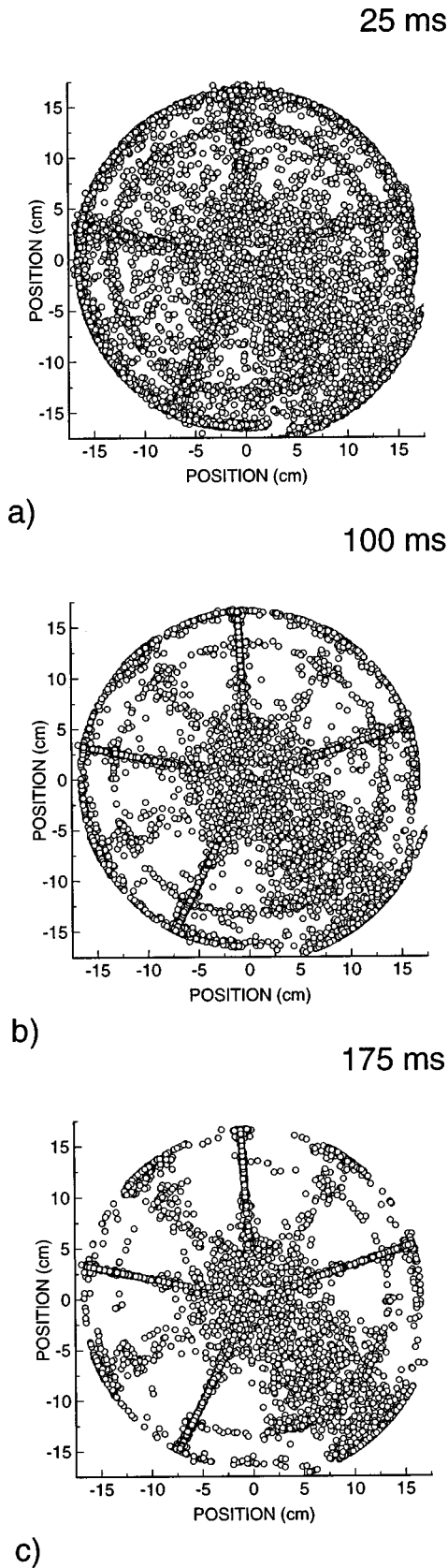
25 ms

a)

100 ms

b)

175 ms

c)

FIG. 5. Plan (or top) views of particle locations (1 μm diameter) in the ICP reactor with nozzles and a load lock bay at various times after release: (a) 25 ms, (b) 100 ms, and (c) 175 ms. Particle trapping occurs in the bulk plasma at azimuths aligned with the nozzles, at midpoints between the nozzles and in front of the load-lock bay.
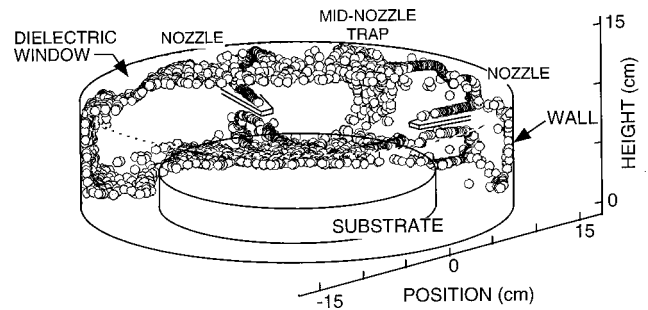

FIG. 6. Cut-away view of particle traps 175 ms after release for the conditions of Fig. 5(c). Particle traps are produced above and below the nozzles, as well as in front of the tip of the nozzle.

with powers of 200 and 500 W. All particle diameters are 1 μm. These particle locations should be compared to the base case (10 mTorr, 100 W) in Fig. 5(c). At 100 mTorr, the traps aligned with the nozzles and at mid-nozzle locations are narrower, a consequence of the temperature of the particles being lower due to the increasing fluid drag. As a result, the particles are confined to a narrower extent of the potential well which forms the trap. Upon increasing power deposition, the ion density increases which increases the ion drag forces, which in turn accelerates particles through the shallow traps. The confining electrostatic fields change little. Note that the traps between the nozzles and in front of the load-lock bay are dispersed at lower powers than those aligned with the nozzles, indicating that their potential depth is smaller.

The configuration of the particle traps is also a function of the size of the particle. Plan views of particle locations at 10 mTorr and 100 W for 400 and 200 nm diam particles are shown in Figs. 8(a) and 8(b). A cut-away view of the particle locations in the vicinity of the nozzles for 400 nm diam particles is shown in Fig. 8(c). Again, compare these results to the base case in Fig. 5(c). As the particle size decreases, the scaling of ion drag versus electrostatic forces for this geometry favors the ion drag forces. The traps between the nozzles are first dispersed, leaving only the traps aligned with the nozzles. The remaining traps are restricted to three distinct locations; above and below the nozzle, and at the tip of the nozzle.

In a prior work, azimuthal asymmetries resulting from transmission line effects in the coils of ICP reactors were discussed.[15] In summary, it was found that poorly terminated coils (or sufficiently long coils that standing waves occur) can produce extrema in the inductively coupled electric field, and hence power deposition, as a function of azimuth. A direct consequence of this asymmetry is the generation of extrema in electron temperature and ionization rates, which produce azimuthally dependent (or side-to-side variations in) ion fluxes to the substrate. Since the ion fluxes are azimuthally asymmetric, then so are the ion generated forces on dust particles. One can then expect that dust particle trapping may be azimuthally asymmetric as well. To investigate this possibility, simulations were performed using HPEM-3D for a solenoid ICP reactor having a three-turn coil, a schematic of
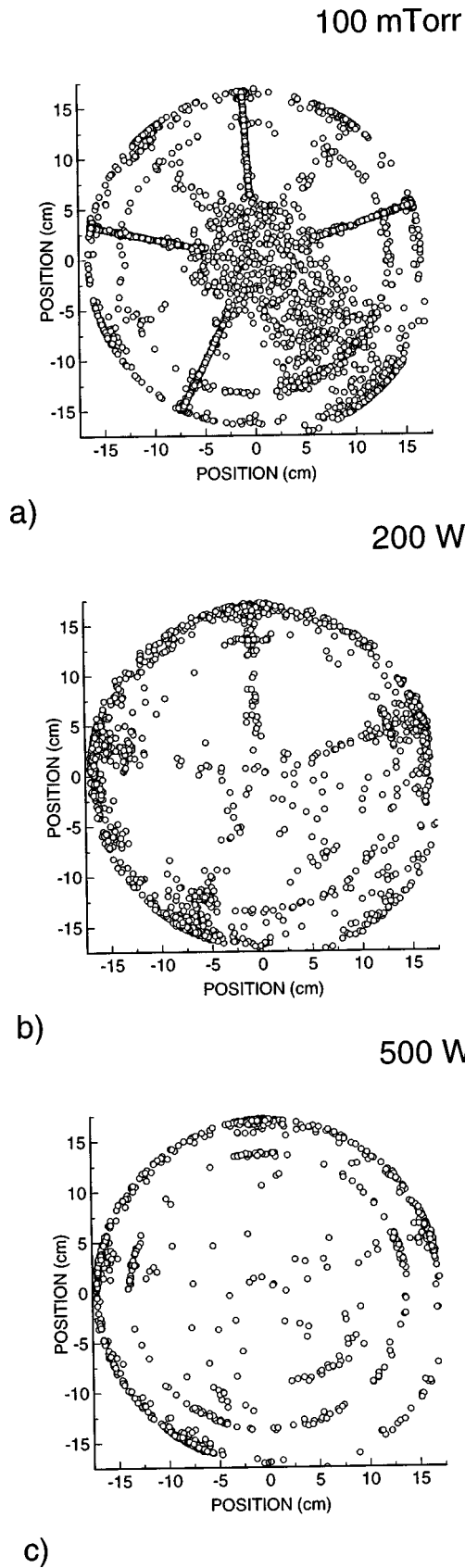
100 mTorr

a)

200 W

b)

500 W

c)

FIG. 7. Plan (or top) views of particle locations while varying plasma operating conditions: (a) 100 mTorr, (b) 200 W power deposition, and (c) 400 W power deposition. Traps are more closely aligned with the nozzles at higher pressure. The traps are dispersed at the higher powers, first at the mid-nozzle locations and load-lock bay, and later at the nozzle locations.

400 nm

a)

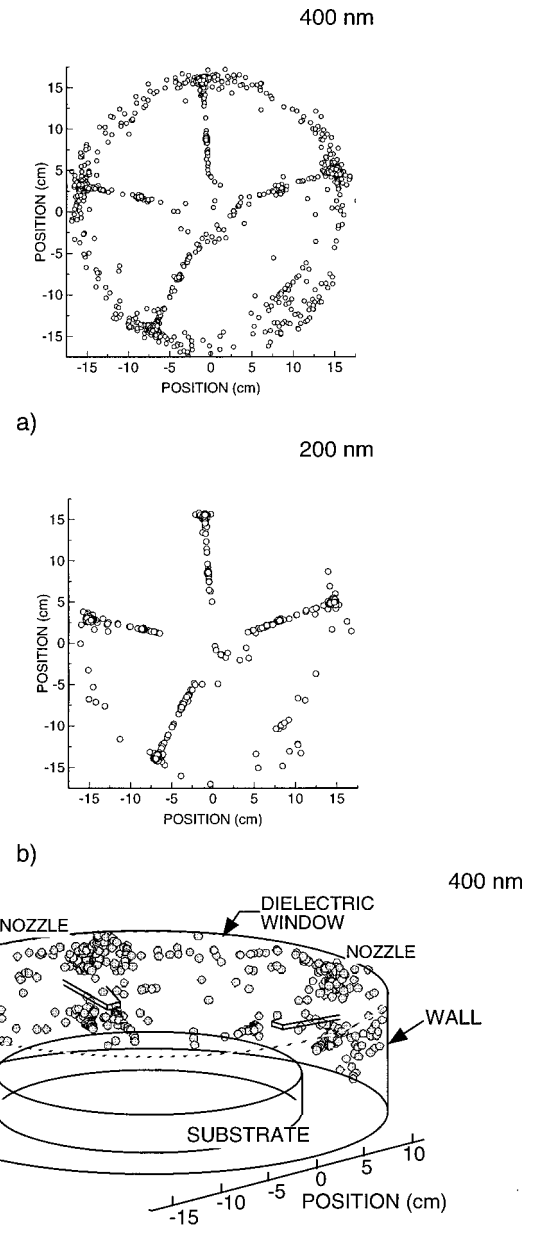## 200 nm

b)

400 nm

c)

FIG. 8. Plan (or top) views of particle locations for: (a) 400 nm and (b) 200 nm diam particles. A cutaway view in (c) shows locations of 400 nm particles. Trapping occurs above and below the nozzles, and at the tip.

which is shown in Fig. 9. The substrate is 20 cm in diameter, and the chamber consists of a dielectric dome having a showerhead nozzle. The operating conditions are Cl_2 at 10 mTorr and 400 W power deposition.

The coil configuration and electrical termination of the solenoid have been purposely chosen to generate an azimuthally asymmetric power deposition. This asymmetry is shown in Fig. 10 where the power deposition is plotted at three elevations in the (r, θ) plane corresponding to approximately the heights of the coils. The Cl_2^+ ion density at approximately the height of the lowest coil is also shown. As a consequence of the poorly matched transmission line charac-
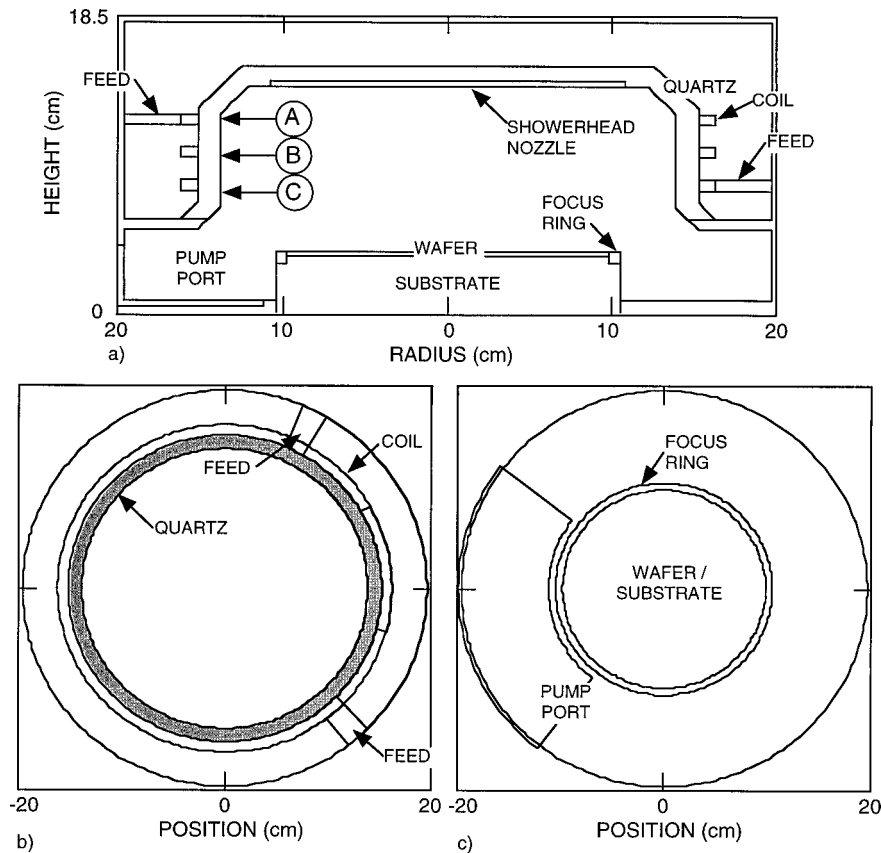
FIG. 9. Schematic of the solenoid coil ICP reactor: (a) side view, (b) (r, θ) slice through the dome showing the coil and feed locations, (c) view looking down on the substrate. The arrows in the top figure indicate the heights at which (r, θ) ''slices'' of plasma properties will be viewed.

teristics of the solenoid, the power deposition is maximum in the lower right third of the reactor (viewed from above) and is a minimum in the lower left third of the reactor. The electron temperature, ionization sources, ion density and plasma potential have maxima and minima following the power deposition. The uniformity of the ion density improves at lower heights, as one moves towards the substrate, where ion diffusion has had an opportunity to repair some of the asymmetry resulting from the nonuniform ion sources at higher heights.

Due to the asymmetry in ion fluxes, which produce the ion drag forces, and the electric potential, which determines the electrostatic forces, the asymmetric power deposition in this reactor could be expected to produce particle traps. This expectation is born out in the results from DTS-3D as shown in Fig. 11. In these plan views, the positions of 1 μm diam particles at 75, 125 and 175 ms after release are shown. A side view of particle positions at 175 ms is shown in Fig. 12. Particles, initially randomly distributed inside the dome, are quickly accelerated by ion drag forces to the walls and periphery of the reactor in the top part of the dome where the power deposition and ion density are largest. The two ''rings'' of particles seen in the plan view at 75 ms correspond to quasi-trapping on the inside of the dome and in the lower outer corner of the reactor beyond the substrate.

As time progresses, the particles in quasi-traps inside the

dome are either driven downward by the diffusing axial ion flux or into the walls of the dome. Particles in the lower left quadrant of the reactor are progressively collected into a trap that extends from the floor of the reactor to the sloped portion of the dome. This extended trap is formed by the local minimum in azimuthal power deposition and ion density, which sufficiently reduces the ion drag forces to enable electrostatic forces to counterbalance the expulsion forces. The trap broadens in azimuth near the bottom of the reactor due to both a decrease in the ion flux and a lowering of the plasma potential. In results for simulations not shown here, the azimuthal location of the particle trap was systematically rotated in angle by changing the termination impedance of the coil. In doing so, the minimum in inductively coupled electric field was shifted to a different location along the transmission line which corresponded to a progressively larger azimuth. As a result, the azimuthal location of the minimum in power deposition and ion density, and the particle trap these minima generate, also rotated to a new azimuth.

IV. CONCLUDING REMARKS

Dust particle trapping in low gas pressure and high plasma density tools is typically not observed in the absence of rf biasing of the substrate due to the dominance of ion
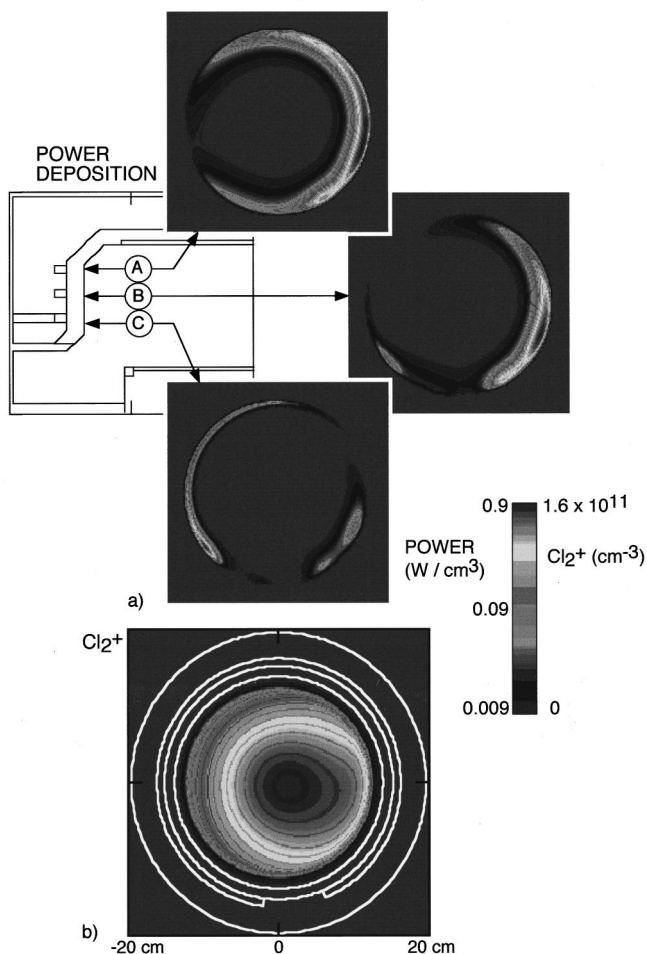
FIG. 10. Plasma properties of the solenoid ICP reactor (10 mTorr Cl_2, 400 W). (a) Power deposition in the (r, θ) plane for heights approximately aligned with the coils. Poor impedance matching produces azimuthal variations. (b) Cl_2^+ density in the (r, θ) plane at height C. The ion density has an azimuthal maximum aligned with the power deposition.

drag forces over electrostatic forces. Results from 3D plasma equipment and dust particle transport models indicate that 3D structures can perturb these forces sufficiently to produce dust particle traps. It was shown that structures such as injection nozzles significantly perturb ion densities and the plasma potential by providing recombination surfaces and a local ground plane. These local reductions in ion drag forces and increase in electrostatic forces are sufficient to produce particle traps both aligned with the nozzles and at the midpoint between the nozzles. These perturbations extend far from the nozzles themselves, and can form extended particle traps. The particle traps are relatively shallow and can be dispersed by increasing power deposition. Electromagnetic 3D structures can also produce particle traps by modulating power deposition and ion density in the plasma. One example of this type of trap is the azimuthally dependent power deposition produced by poor impedance matching of a long coil of a solenoid reactor. Ion drag forces are reduced at the azimuth corresponding to the minimum in power deposition, thereby producing a broad particle trap.
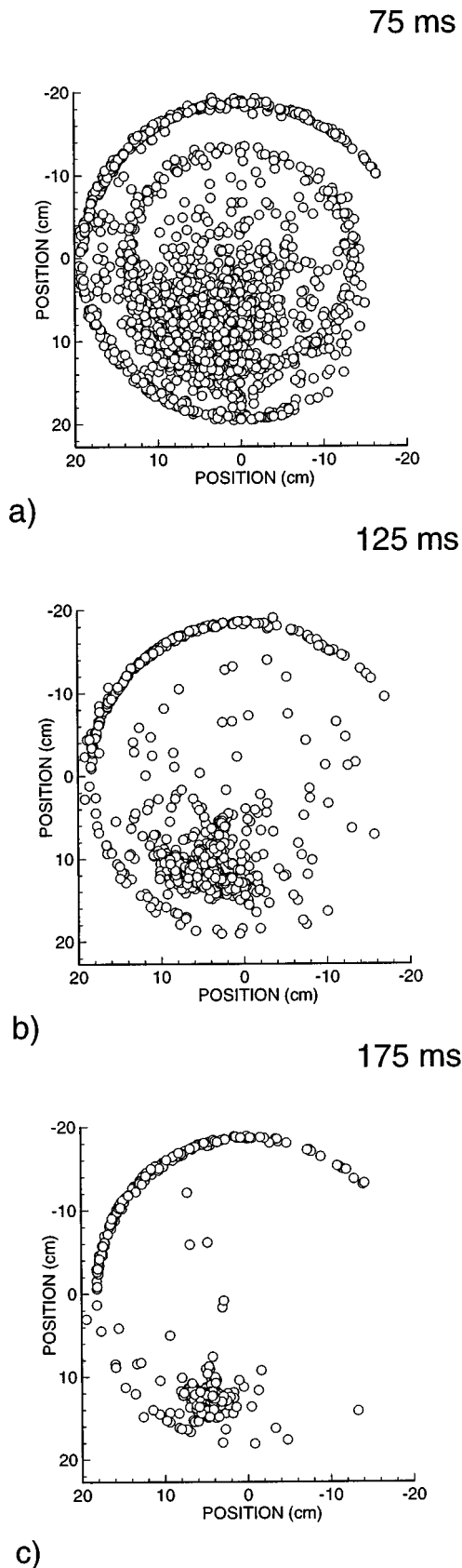

FIG. 11. Plan (or top) views of particle locations (1 μm diameter) in the solenoid ICP reactor at various times after release: (a) 75 ms, (b) 125 ms, and (c) 175 ms. Particle trapping occurs at the azimuth corresponding to the minimum in power deposition.
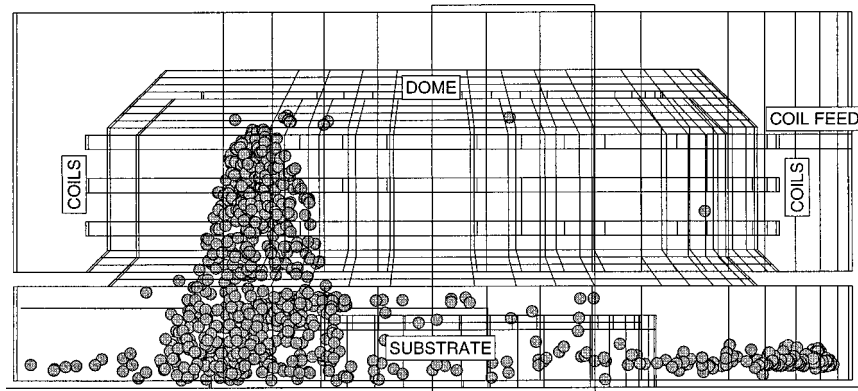
FIG. 12. Side view of particle locations at 175 ms for the conditions of Fig. 11. The particle trap extends from the bottom of the reactor into the dome, narrowing at larger heights.

[1] A collection of papers addressing particle transport in plasma processing reactors appears in two recent special issues of journals: Plasma Sources Sci. Technol. **3**, 239 (1994); J. Vac. Sci. Technol. A **14**, 489 (1996).

[2] J. B. Pieper, J. Goree, and R. A. Quinn, J. Vac. Sci. Technol. A **14**, 519 (1996).

[3] H. H. Hwang and M. J. Kushner, J. Appl. Phys. **82**, 2106 (1997).

[4] G. S. Selwyn, Plasma Sources Sci. Technol. **3**, 340 (1994).

[5] M. Dalvie, M. Surendra, G. S. Selwyn, and C. R. Guarnieri, Plasma Sources Sci. Technol. **3**, 442 (1994).

[6] J. E. Daugherty and D. B. Graves, J. Appl. Phys. **78**, 2279 (1995).

[7] D. B. Graves, J. E. Daugherty, M. D. Kilgore, and R. K. Porteous, Plasma Sources Sci. Technol. **3**, 443 (1994).

[8] G. S. Selwyn and A. D. Bailey III, J. Vac. Sci. Technol. A **14**, 634 (1996).

[9] S. M. Collins, D. A. Brown, J. F. O'Hanlon, and R. N. Carlile, J. Vac. Sci. Technol. A **14**, 649 (1996).

[10] H. H. Hwang and M. J. Kushner, Appl. Phys. Lett. **68**, 3716 (1996).

[11] D. P. Lymberopoulos and D. J. Economou, J. Res. Natl. Inst. Stand. Technol. **100**, 473 (1995).

[12] R. A. Stewart, P. Vitello, D. B. Graves, E. F. Jaeger, and L. A. Berry, Plasma Sources Sci. Technol. **4**, 36 (1995).

[13] G. Dipeso, V. Vahedi, D. W. Hewett, and T. D. Rognlien, J. Vac. Sci. Technol. A **12**, 1387 (1994).

[14] D. L. Lymberopoulos and D. Economou, IEEE Trans. Plasma Sci. **23**, 573 (1995).

[15] M. J. Kushner, W. Z. Collison, M. J. Grapperhaus, J. P. Holland, and M. S. Barnes, J. Appl. Phys. **80**, 1337 (1996).

[16] M. J. Kushner, J. Appl. Phys. **82**, 5312 (1997).